7448 *Biochemistry* **2010,** *49,* 7448–7458
DOI: 10.1021/bi100768g

BIOCHEMISTRY
including biophysical chemistry & molecular biology
Article

Ligand Migration and Binding in Nonsymbiotic Hemoglobins of *Arabidopsis thaliana*[†]

Karin Nienhaus,[‡] Paola Dominici,[§] Alessandra Astegno,[§] Stefania Abbruzzetti,[∥] Cristiano Viappiani,[∥] and G. Ulrich Nienhaus*[,‡,⊥]

[‡]*Institute of Applied Physics and Center for Functional Nanostructures, Karlsruhe Institute of Technology, 76128 Karlsruhe, Germany,* [§]*Dipartimento di Biotecnologie, Università degli Studi di Verona, Verona, Italy,* [∥]*Dipartimento di Fisica, Università degli Studi di Parma, NEST CNR-INFM, Parma, Italy, and* [⊥]*Department of Physics, University of Illinois, 1110 West Green Street, Urbana, Illinois 61801*

Received May 14, 2010; Revised Manuscript Received July 25, 2010

ABSTRACT: We have studied carbon monoxide (CO) migration and binding in the nonsymbiotic hemoglobins AHb1 and AHb2 of *Arabidopsis thaliana* using Fourier transform infrared (FTIR) spectroscopy combined with temperature derivative spectroscopy (TDS) at cryogenic temperatures. Both proteins have similar amino acid sequences but display pronounced differences in ligand binding properties, at both physiological and cryogenic temperatures. Near neutral pH, the distal HisE7 side chain is close to the heme-bound ligand in the majority of AHb1-CO molecules, as indicated by a low CO stretching frequency at 1921 cm^{-1}. In this fraction, two CO docking sites can be populated, the primary site B and the secondary site C. When the pH is lowered, a high-frequency stretching band at ~1964 cm^{-1} grows at the expense of the low-frequency band, indicating that HisE7 protonates and, concomitantly, moves away from the bound ligand. Geminate rebinding barriers are markedly different for the two conformations, and docking site C is not accessible in the low-pH conformation. Rebinding of NO ligands was observed only from site B of AHb1, regardless of conformation. In AHb2, the HisE7 side chain is removed from the bound ligand; rebinding barriers are low, and CO molecules can populate only primary docking site B. These results are interpreted in terms of differences in the active site structures and physiological functions.

The flowering plant *Arabidopsis thaliana* is a dicot from the mustard family that has been widely used as a model organism in studies of plant development. In 1997, two hemoglobins (Hbs)[1] from *A. thaliana*, AHb1 and AHb2, were cloned and characterized (*1*). AHb1 was assigned to the class 1 family of nonsymbiotic Hbs previously found in a number of plant species (*2*, *3*), whereas AHb2 belongs to the nonsymbiotic Hbs of class 2 (*4*), which share similarities with symbiotic Hbs of legumes and *Casuarina* evergreens (*1*). AHb1 expression is induced in roots and rosette leaves by low dioxygen (O_2) levels; AHb2 expression is restricted to rosette leaves and induced by low temperatures (*5*). The two Hbs also differ markedly in their ligand binding properties, suggesting different physiological roles. AHb1 has an extremely high O_2 affinity that excludes a function as an O_2 carrier. It has been proposed to be a NO dioxygenase, instead (*6*). By contrast, AHb2 displays a moderate oxygen affinity, but likewise, a function as an O_2 carrier appears unlikely because of its unusually low O_2 off rate (*1*).[1]

Equilibrium and kinetics of ligand binding to heme proteins are governed by structural properties of the active site, the availability of ligand docking sites within the protein matrix, and pathways for ligand migration between internal sites and the solvent environment. Two key residues, B10 and E7 (in myoglobin residue numbering), at the active site strongly modulate ligand binding to Hbs. The leucine B10/histidine E7 (LeuB10/HisE7) amino acid pair, predominantly found in vertebrate oxygen storage and transport proteins, appears optimally suited for reversible binding of O_2 (*7*, *8*). Other members of the globin family carry the tyrosine B10/glutamine E7 (TyrB10/GlnE7) combination at the active site; among these are the truncated Hbs (*5*). O_2 affinities in this subfamily are typically too high to allow for reversible ligand binding in an O_2 transport protein, due to the strong stabilization of the heme-bound O_2 by both GlnE7 and TyrB10. However, this pair of residues appears well suited for NO scavenging and detoxification (*9*). Plant Hbs including AHb1 and AHb2 have phenylalanine B10/histidine E7 (PheB10/HisE7) in their distal pockets (*10*).

In the exploration of structure−function relations in heme proteins, X-ray crystallography has provided a wealth of structural information, yet even at a very high resolution, local structural details of active sites, including the presence of subconformations, are difficult to determine accurately. Spectroscopic methods such as X-ray, optical, and vibrational absorption spectroscopies probe only local features but are often exquisitely sensitive to the finest structural details (*11*−*15*). The interpretation of spectroscopic markers in structural terms is not straightforward, however, and usually requires substantial efforts in theoretical calculations (*14*, *16*−*22*). In our group, we have extensively employed CO and NO ligands in heme proteins as local structural probes using Fourier transform infrared (FTIR) spectroscopy, often combined with temperature derivative spectroscopy (TDS), to learn a great deal about active site structures and interactions in heme proteins (*23*−*26*). The strong infrared absorption of the heme-bound CO ligand is sensitive to the electric field at the binding site due to the vibrational Stark effect

[†]This work was supported by the Deutsche Forschungsgemeinschaft (DFG NI291/3 and CFN) and the Fonds der Chemischen Industrie (to GUN).

*To whom correspondence should be addressed. E-mail: uli@uiuc.edu. Phone: +49 (0)721 608 3401. Fax: +49 (0)721 608 8480.

[1]Abbreviations: AHb, *A. thaliana* hemoglobin; FTIR, Fourier transform infrared; TDS, temperature derivative spectroscopy; Mb, myoglobin; Hb, hemoglobin.

 Published on Web 07/28/2010

(VSE) (*27*−*30*), and thus an excellent probe of local structure. In CO-ligated wild-type (wt) myoglobin (MbCO), multiple-CO group stretching gave clear evidence of a discrete set of active site conformations (*31*) long before their individual structures were revealed by X-ray crystallography (*32*, *33*). The CO stretching spectrum of wt MbCO at pH 7 shows two main bands, A_1 at 1945 cm^{-1} and A_3 at 1930 cm^{-1} (*24*). A third band emerges at 1965 cm^{-1} only at low pH, representing the A_0 conformation, in which the HisE7 side chain is protonated [pK_a = 4.5 (*34*)] and rotated toward the solvent to screen the charge (*32*). The upshifted frequency of A_0 indicates a lack of interaction between the HisE7 imidazole and the heme-bound CO. Accordingly, A_0-like stretching bands are observed upon replacement of HisE7 with amino acids with aliphatic side chains (*13*, *35*). In both the A_1 and A_3 conformations, the hydrogen on Nε of the neutral HisE7 donates a hydrogen bond and, thereby, stabilizes the bound ligand, which is crucially important for the protein's O_2 binding function. The HisE7-NεH moiety is positioned slightly closer to the bound ligand in the A_3 conformation than in A_1 (*33*) and, consequently, causes a larger red shift of its stretching band (*13*, *31*). A_3-like stretching bands are enhanced in mutant Mbs with either phenylalanine (*13*, *36*) or tyrosine (*37*) at position B10.

CO ligands can be photodissociated efficiently from the heme iron (*38*). However, at temperatures below ~160 K, large-scale protein motions are arrested (*39*, *40*), and ligands cannot escape into the solvent. Trapped inside the protein matrix, they frequently accumulate in structurally well-defined docking sites, where they give rise to characteristic stretching bands between 2100 and 2160 cm^{-1} (*24*, *25*). Often, a doublet of IR bands is observed because the CO can reside in such a site in opposite orientations (*41*), because of vibrational Stark splitting of the CO stretching band in the presence of a local electric field (*14*, *27*, *42*).

The X-ray structures of AHb1 and AHb2 have not yet been determined. To gain insight into the small structural differences between these very similar proteins that give rise to markedly different ligand binding properties, we have conducted FTIR-TDS experiments on these proteins. By using specific sample illumination protocols at cryogenic temperatures (*43*−*45*), we were able to characterize and selectively populate ligand docking sites and to observe ligand migration between them.

MATERIALS AND METHODS

Protein Expression and Purification. AHb1 and AHb2 were cloned, expressed, and purified as described previously (*46*). The coding sequence for AHb1, cloned into vector pGEM-T Easy (Promega, Madison, WI), was used as a template to introduce point mutations PheB10Leu and HisE7Leu using the Quik-Change II mutagenesis kit (Stratagene, La Jolla, CA). Mutants were expressed and purified as described for the wt protein (*46*).

FTIR Absorption Spectroscopy. A concentrated protein solution in 75%/25% (v/v) glycerol/buffer (potassium phosphate) cryosolvent was equilibrated with 1 atm of CO for 1 h. A 2-fold molar excess of sodium dithionite was added anaerobically before the mixture was stirred for an additional 15 min under a CO atmosphere. The sample solution was centrifuged at 5000 rpm (Eppendorf table top centrifuge) for 15 min prior to being loaded into the sample cell to remove any undissolved protein.

A few microliters of the protein solution was kept between two CaF_2 windows (diameter of 25.4 mm) separated by a 75 μm thick mylar washer. The windows were sandwiched inside a block of oxygen-free high-conductivity copper mounted on the coldfinger of a closed-cycle helium refrigerator (model SRDK-205AW, Sumitomo, Tokyo, Japan). The sample temperature was measured with a silicon temperature sensor diode and regulated with a digital temperature controller (model 330, Lake Shore Cryotronics, Westerville, OH). Samples were photolyzed by a continuous wave, frequency-doubled Nd:YAG laser (model Forte 530-300, Laser Quantum, Manchester, U.K.), emitting an output power of 300 mW at 532 nm. The laser beam was split and focused with lenses on the sample from both sides. We collected Fourier transform infrared (FTIR) transmission spectra in the mid-infrared region between 1800 and 2400 cm^{-1} at a resolution of 2 cm^{-1} (IFS 66v/S, Bruker, Karlsruhe, Germany).

FTIR absorption spectra were calculated from transmission spectra, $I(\nu)$, of the ligated (CO or NO) and the aquomet derivative of the same protein preparation $\{A(\nu) = \log[I_{met}(\nu)/I_{light}(\nu)]\}$. Photolysis difference spectra were calculated from transmission spectra collected before and after photolysis $[\Delta A = \log(I_{dark}/I_{light})]$. Consequently, difference bands of heme-bound CO (1900−2000 cm^{-1}) display a negative amplitude because they are missing after photolysis. Photoproduct bands (2100−2160 cm^{-1}) are created by photolysis and thus have positive amplitudes.

Temperature Derivative Spectroscopy (*TDS*). Temperature derivative spectroscopy (TDS) is an experimental protocol designed for the investigation of thermally activated rate processes with distributed enthalpy barriers (*43*, *47*, *48*). Initially, a nonequilibrium state has to be created, at a temperature at which approach to equilibrium is negligible. This is most often done by photodissociation of the ligand. Subsequently, FTIR transmission spectra, $I(\nu,T)$, are taken every 1 K while the sample temperature T is increased at a constant rate of 0.3 K/min. Ligand rebinding causes a change in the spectral area during acquisition of two successive spectra. The temperature ramp protocol ensures that rebinding occurs sequentially with respect to the height of the activation enthalpy barrier that opposes ligand rebinding. A quantitative kinetic analysis has to consider both (i) the change in absorbance due to rebinding and (ii) a possible intrinsic temperature dependence of the measured spectra (*27*, *49*, *50*). We present FTIR-TDS data as two-dimensional contour plots on a surface spanned by the temperature and wavenumber axes, with black (red) lines indicating an absorbance increase (decrease) and contours spaced logarithmically.

Illumination Protocols. To selectively populate ligand docking sites, we have utilized two different illumination protocols. In one case, the sample is illuminated briefly (1−10 s) at 4 K to achieve complete photolysis of the sample. The subsequent TDS experiment records rebinding from photoproduct states that can be populated at 4 K. However, some docking sites may be accessible only upon photodissociation at higher temperatures due to higher barriers on the ligand migration pathway. To trap ligands in such states, we use the slow-cool protocol. The sample is illuminated by the actinic laser light while it is cooled (typically from 160 to 4 K). At 160 K, escape of ligand from the protein is still negligible so that, after photodissociation, they rebind quickly and are photolyzed again. Because the temperature is continuously decreased, rebinding will become progressively slower. At one point, ligands that explore remote sites separated from the active sites by higher barriers cannot return to the heme iron any more and become trapped in these sites. Subsequently, ligands that have not yet been trapped may migrate to other

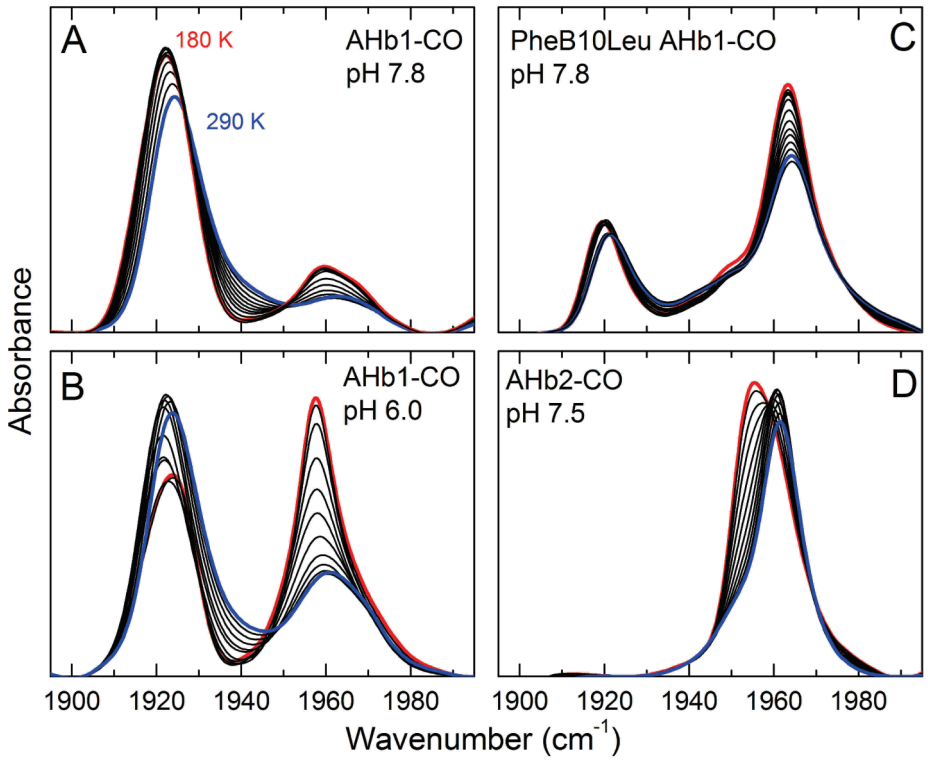

FIGURE 1: Temperature dependence of the FTIR absorption spectra of (A) AHb1-CO at pH 7.8, (B) AHb1-CO at pH 6.0, (C) PheB10Leu AHb1-CO at pH 6.0, and (D) AHb2-CO at pH 7.5. The temperature interval was from 180 to 290 K, in 10 K steps: (blue line) 290 K and (red line) 180 K.

docking sites with smaller energy barriers and will also be trapped. The slow-cool approach is, therefore, convenient in screening for possible intermediate sites.

RESULTS AND DISCUSSION

Structural Heterogeneity at the Active Sites of AHb1-CO and AHb2-CO. Figure 1 displays FTIR difference spectra of AHb1-CO, PheB10Leu AHb1-CO, and AHb2-CO in the temperature range of 180−290 K. AHb1-CO at pH 7.8 displays a dominant band at 1924 cm^{-1}, termed A_{1924} in the following, and a minor one at 1964 cm^{-1} (Figure 1A). The bands sharpen with a decrease in temperature; the minority population can be decomposed into two bands at 1959 and 1968 cm^{-1}. When the pH is lowered, A_{1959} gains amplitude at the expense of A_{1924} (Figure 1B). This effect is significantly enhanced at the lower temperature, as was also observed for the A_0 band of MbCO (*35*). By contrast, the band at 1968 cm^{-1} remains weak and is barely noticeable at a low pH and temperature. In mutant PheB10Leu AHb1-CO (Figure 1C), the band at ~1960 cm^{-1} dominates the spectrum at 290 K and is even more intense at 180 K. AHb2-CO displays only a single band at ~1960 cm^{-1} (Figure 1D), which shifts from 1962 (290 K) to 1955 cm^{-1} (at 180 K).

Photolysis difference spectra, calculated from transmission spectra taken before and after 10 s laser illumination at 4 K, are plotted in Figure 2A. To achieve essentially complete photolysis of both AHb1-CO and AHb2-CO, illumination for 10 s was necessary, whereas 1 s is entirely sufficient in our experimental setup to completely photolyze MbCO. As the quantum yield of photodissociation is ~1, this result suggests that a major fraction of photolyzed ligands in AHb are not efficiently trapped in their docking sites and recombine instead, so that multiple trials are necessary to form a stable photoproduct.

In the 4 K difference spectra at pH 7.8, AHb1-CO displays a dominant stretching band of heme-bound CO at 1921 cm^{-1} (Figure 2A, black line); weaker bands are present at 1959 and 1968 cm^{-1}. At pH 6.0, A_{1921} has lost population to A_{1959} (Figure 2A, green line); A_{1968} is still only a minority species. The photolysis difference spectrum of the isoelectronic ferric AHb1-NO, at pH 7.6, displays a prominent band at 1920 cm^{-1}

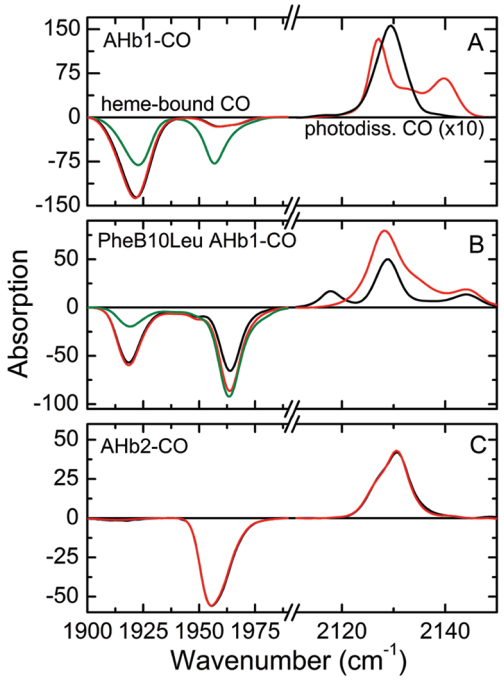

FIGURE 2: FTIR photolysis difference spectra of (A) AHb1-CO, (B) PheB10Leu AHb1-CO, and (C) AHb2-CO at 4 K, color-coded according to the chosen illumination protocol: black for 10 s illumination at 4 K, red for slow-cool illumination from 160 to 4 K (sample pH of ~7.5), and green for slow-cool illumination from 160 to 4 K (sample pH of ~6).

Table 1: IR Stretching Band Frequencies of Heme-Bound and Photodissociated CO Determined at 4 K after a 10 s Illumination at 4 K and after Slow-Cool Illumination from 160 to 4 K[a]

sample	pH	ν(heme-bound CO, 10 s) (cm^{-1})	ν(photodissociated CO, 10 s) (cm^{-1})	ν(photodissociated CO, slow cool) (cm^{-1})
AHb1-CO	7.8	1921 (89), 1959 (7), 1968 (4)	2118 (1), 2122 (3), 2129 (94), 2138 (2)	2127 (36), 2129 (14), 2134 (21), 2140 (29)
AHb1-CO	6.0	1921 (53), 1957 (40), 1969 (7)	−	2127 (21), 2129 (35), 2134 (21), 2140 (23)
PheB10Leu AHb1-CO	7.5	1919 (40), 1950 (7), 1964 (53)	2118 (19), 2129 (54), 2135 (7), 2144 (20)	2121 (3), 2128 (64), 2135 (16), 2144 (17)
AHb2-CO	7.8	1955 (65), 1963 (35)	2126 (28), 2131 (67), 2138 (5)	2126 (28), 2131 (67), 2138 (5)

[a]Values in parentheses represent the fraction of the total in percent. Estimated experimental error of ±0.5 cm^{-1}.

and a smaller one at 1902 cm^{-1}, indicating that two subconformations also coexist in the NO-ligated state (Figure S1 of the Supporting Information). In mutant PheB10Leu AHb1-CO, two bands at 1919 and 1964 cm^{-1} contribute almost equally to the spectrum at pH 7.8; a minor band is seen at 1950 cm^{-1} (Figure 2B, black line). When the pH is lowered to 5.8, A_{1964} gains intensity at the expense of A_{1919} (Figure 2B, green line). The spectrum of AHb2-CO at pH 7.8 shows a single asymmetric peak that can be fitted by two Gaussian bands at 1955 and 1963 cm^{-1} (Figure 2C). A weak band at ~1910 cm^{-1} is due to the ^{13}CO isotope. All peak positions obtained by fitting Gaussian bands to the spectra are compiled in Table 1.

The stretching spectra of heme-bound CO provide clear evidence that the active sites of AHb1 and AHb2 are structurally distinctly different. In AHb2, the high frequency of the CO stretching absorption is typical of an apolar CO environment and indicates that the HisE7 side chain does not interact with the bound CO. This result is corroborated by the low, 490 cm^{-1} frequency of ν_{FeC} seen in resonance Raman spectra (*46*). The ν_{FeC} and ν_{CO} frequencies are inversely correlated, due to d_π electron back-donation from the iron to the CO ligand (*13*, *15*, *51*). In Mb, the high-frequency, A_0 conformation is achieved by HisE7 imidazole protonation and concomitant reorientation toward the solvent. Comparison of the X-ray structures of hexacoordinated rice Hb1 and CN-ligated barley Hb suggests that protonation and HisE7 side chain reorientation are not required to abolish its interaction with the bound CO ligand (*52*). Instead, ligand binding is accompanied by a large shift of helix E along the helical axis that displaces the HisE7 side chain from the bound ligand by several angstroms.

In contrast, the CO spectrum of AHb1-CO is dominated by the A_3-like stretching band A_{1921}, implying that the NεH group of HisE7 interacts strongly with the heme-bound CO, unlike in the minor A_{1959} and A_{1968} conformations. The fraction of A_{1959} in the CO spectrum increases when the pH is lowered, which, as is well-known for MbCO (*32*, *34*), indicates an A_0-type conformation. These findings also agree with room-temperature resonance Raman experiments with the CO complex of AHb1 (*46*). For wt AHb1-CO, bands at 533 and 1923 cm^{-1} were assigned to the ν_{FeC} and ν_{CO} modes, respectively, on the basis of $^{12}C/^{13}C$ isotopic substitution. High ν_{FeC} frequencies in combination with low ν_{CO} frequencies signal a polar environment of the bound CO (*53*). The ν_{FeC} and ν_{CO} bands at 501 and 1964 cm^{-1} in mutant AHb1-CO HisE7Leu indicate a reduced polarity in the distal cavity in this variant, thus confirming that HisE7 is the residue that places a positive partial charge near the heme-bound CO in wt AHb1 (*54*). The lower frequency of A_{1959} in comparison with that of the A_0 conformation of MbCO at 1966 cm^{-1} (*48*, *55*) likely arises from the presence of the phenylalanine side chain close to the bound CO.

The high frequency of the minority band A_{1968} indicates a weak electrostatic interaction of the CO in the heme pocket, but its pH dependence implies that the HisE7 side chain is not protonated and thus resides in the heme pocket. A weakly populated subconformation with these properties was also found in MbCO and assigned to the neutral $H64^{\varepsilon 2,180}$ conformation (*34*), in which the imidazole is protonated at Nε but rotated by 180° so that the hydrogen on Cε is proximal to the CO. Oldfield and co-workers (*56*) showed that this conformation interacts minimally with the CO. They erroneously assigned A_0 to this conformation because they did not consider HisE7 protonation, and the structural changes associated with A_0 had not yet been determined (*32*). Kushkuley and Stavrov (*19*) also calculated only a small blue shift for this species (3.5 cm^{-1}).

Replacement of PheB10 with Leu in AHb1 significantly increases the relative population in the A_0-like conformation A_{1964} (Figure 2B); ~50% of the molecules remain in an A_3-like conformation, with a stretching frequency that is even lower than that of the wt protein (Figure 2B). This result agrees with observations made with room-temperature resonance Raman spectra (*54*). Comparable changes in the ratio of the A_0- and A_3-like subconformations have also been reported upon replacement of PheB10 with Leu in murine neuroglobin (Ngb) (*36*) and nonsymbiotic rice Hb1 (*57*). Apparently, the presence of the bulky PheB10 leads to a marked stabilization of the A_3-like conformation in which the HisE7 side chain resides in the heme pocket. In agreement with this conclusion, replacement of LeuB10 with Phe in MbCO (pH 7) leads to a substantial stabilization of the A_3 substate (*36*). In addition to this effect, a small additional band emerges in the AHb1 spectra at 1950 cm^{-1}, which may represent A_1-like molecules, with the HisE7 slightly farther from the bound CO as compared to A_3.

CO at Primary Docking Site B. After illumination for a few seconds at 4 K, photolyzed CO ligands in heme proteins are predominantly trapped in primary docking site B near the heme iron (*58*−*60*). After photolysis of AHb1-CO (pH 7.8), CO ligands at site B give rise to a dominant photoproduct band at 2128 cm^{-1}; additional small bands are present at 2118, 2122, and 2138 cm^{-1} (Figure 2A and Table 1). The photoproduct spectrum of PheB10Leu AHb1-CO at pH 7.5 can be modeled with four bands at 2118, 2128, 2135, and 2144 cm^{-1} (Figure 2B). The photoproduct band of AHb2-CO is asymmetric, with a shoulder on the low-frequency side, and can be modeled by two bands at 2126 and 2131 cm^{-1} (Figure 2C).

Ligand rebinding from site B is observed in TDS experiments started immediately after a 10 s illumination at 4 K. Contour maps for AHb1-CO (pH 7.8) are plotted in Figure 3A,B. Rebinding in the A_{1921} band begins at ~30 K, peaks at ~65 K, and extends beyond 100 K. The absorption increase at 1921 cm^{-1} is accompanied by a loss in the photoproduct band at 2128 cm^{-1}, confirming that CO ligands contributing to B_{2128} rebind to the conformation associated with A_{1921} (Figure 3B). In the high-frequency bands of AHb1-CO, A_{1959} and A_{1968}, ligands start to rebind from site B already at the lowest temperatures, with maxima at 15 and 50 K. The process is completed at ~80 K.

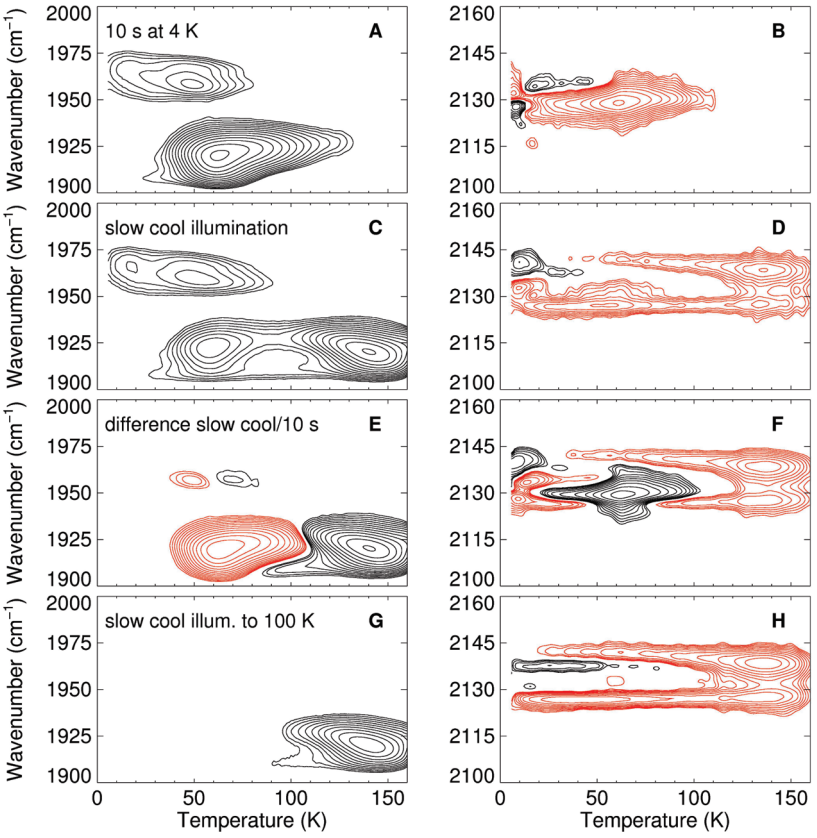

FIGURE 3: TDS contour maps of AHb1-CO at pH 7.8. Data were recorded (A and B) after a 10 s illumination at 4 K, (C and D) after a slow cooling from 160 to 4 K under continuous illumination, and (G and H) after a slow cooling from 160 to 100 K under continuous illumination and cooling to 4 K in the dark. (A, C, and G) Absorption changes in the bands of heme-bound CO. (B, D, and H) Absorption changes in the photoproduct bands. Contours are spaced logarithmically; black and red lines represent increasing and decreasing absorption, respectively. (E and F) Difference contour maps calculated from the data in panels A and C and panels B and D, respectively.

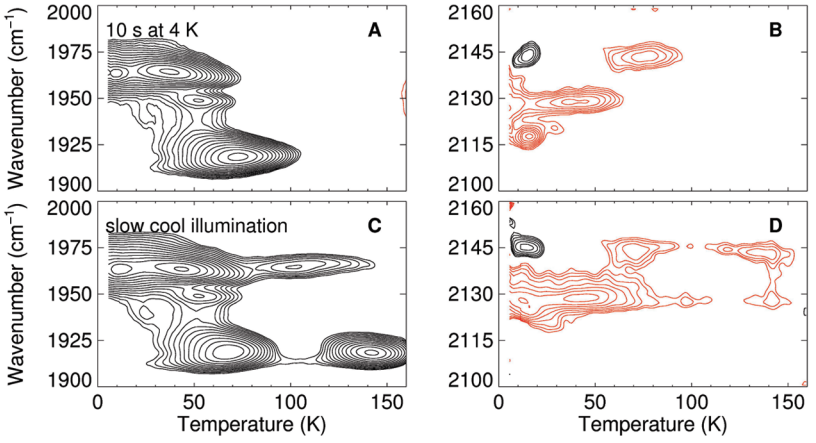

FIGURE 4: TDS contour maps of PheB10Leu AHb1-CO. Data were recorded (A and B) after a 10 s illumination at 4 K and (C and D) after a slow cooling from 160 to 4 K under continuous illumination. (A and C) Absorption changes in the bands of heme-bound CO. (B and D) Absorption changes in the photoproduct bands. Contours are spaced logarithmically; black and red lines represent increasing and decreasing absorption, respectively.

The small population leads to very small photoproduct bands that cannot be separated from the features of the dominant B_{2128} population in the contour map.

In mutant PheB10Leu AHb1-CO, ligands rebind at 70 K in A_{1919} (Figure 4A) after a brief 4 K illumination. In the photoproduct map (Figure 4B), the band at 2145 cm^{-1} loses intensity with the same temperature dependence as A_{1919}, so it is clear that these photodissociated CO ligands absorb at 1919 cm^{-1} after rebinding. The similarly shaped red and black features peaking at 15 K indicate a population exchange between two photoproduct species, B_{2118} and B_{2145}, and not rebinding. Apparently, HisE7 produces a strong VSE splitting of 27 cm^{-1} when the protein is in the A_{1919} conformation, and the CO fraction contributing to B_{2118} reorients within site B before subsequently rebinding at ~70 K. Rebinding in A_{1964} occurs in two steps, with maxima at 5 and 35 K (Figure 4A). The amplitude loss of the photoproduct band at 2130 cm^{-1} has the corresponding temperature dependence (Figure 4B), suggesting that ligands contributing to the 2130 cm^{-1} band rebind in A_{1964}. As the HisE7 side chain is rotated out of the pocket in A_{1964}, the Stark splitting is absent (*14*).

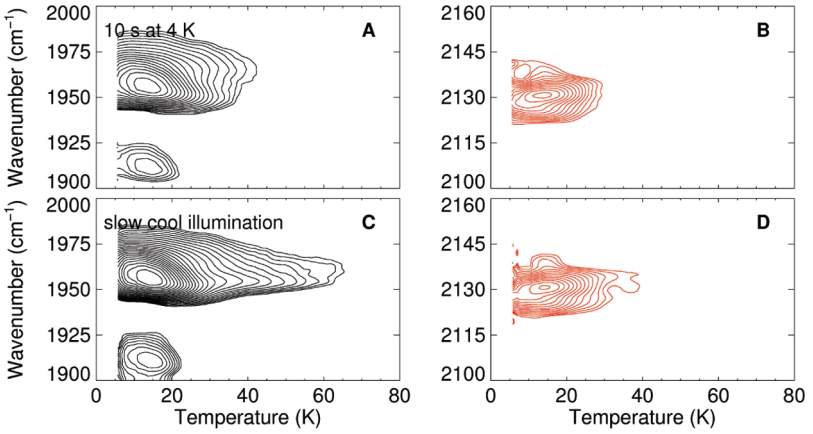

FIGURE 5: TDS contour maps of AHb2-CO. Data were recorded (A and B) after a 10 s illumination at 4 K and (C and D) after a slow cooling from 160 to 4 K under continuous illumination. (A and C) Absorption changes in the bands of heme-bound CO. (B and D) Absorption changes in the photoproduct bands. Contours are spaced logarithmically; black and red lines represent increasing and decreasing absorption, respectively.

The results obtained with PheB10Leu AHb1-CO raise the question of why such a strong VSE splitting occurs in this mutant, but not in the photoproduct spectrum of A_{1921} in wt AHb1-CO. Indeed, the mutant behaves like MbCO, where the low-frequency, A_3 band is also associated with a strongly split photoproduct doublet (*49*). The low stretching frequency of the heme-bound CO implies a strong interaction with the bound ligand. Upon photolysis at 4 K, we do not expect major displacements of the HisE7 side chain because large-scale protein dynamics is arrested (*39*, *40*). The observation that HisE7 in wt AHb1-CO apparently does not lead to a strongly split Stark doublet of photoproduct bands suggests that the photodissociated CO in wt AHb1 is trapped at a position different from that in PheB10Leu AHb1 and MbCO, so that it does not sense the presence of HisE7. Support for this assertion comes from recent studies of ligand migration in carbonmonoxy neuroglobin (NgbCO), where it was shown that the PheB10 side chain actually splits the primary docking site into two sites, B′ and B″, with B′ remote from HisE7 (*61*, *62*). In molecular dynamics simulations of photodissociated NgbCO, ligands migrated only to site B′, in which a small Stark splitting was observed experimentally and by theoretical calculations of the spectra based on the simulations; B″ was not populated. In NgbCO mutant PheB10Leu, CO ligands were observed in site B″; the photoproduct spectra displayed additional bands, and the overall spectrum covered a much wider frequency range.

Rebinding in AHb2-CO peaks at ~25 K, as seen in the contour map of the heme-bound CO (Figure 5A) and from the loss of the corresponding photoproduct band at ~2130 cm^{-1} (Figure 5B). As for A_{1959} of AHb1, a Stark splitting of the band is absent. We note that the contours at ~1910 cm^{-1} in Figure 5A represent rebinding of ^{13}CO in A_{1955} rather than a different conformation. This band is enhanced because of the logarithmic contour level spacing but hardly visible in the photolysis difference spectra in Figure 2C.

CO rebinding in the A_3 conformations of wt and mutant PheB10Leu AHb1 proteins occurs at much higher temperatures than in A_0. With the Arrhenius prefactor ($A = 10^{9.4}$ s^{-1}) from flash photolysis experiments on AHb1-CO in the visible region at cryogenic temperatures (data not shown), we can estimate the peak enthalpies of the barrier distributions that describe rebinding from site B (*47*, *48*). We note that the prefactors vary a bit between the different A states (*55*, *63*), and experiments in the visible average over these effects. For A_3 of wt AHb1, the TDS data can be modeled with two Gaussian barrier distributions, with a ΔH_{peak1} of 13.5 kJ/mol and a ΔH_{peak2} of 18.3 kJ/mol. For A_3 of AHb1 mutant PheB10Leu, the temperature dependence of rebinding can be modeled with a single enthalpy barrier distribution, with a ΔH_{peak} of 15.9 kJ/mol. In contrast, recombination in A_0 molecules of both AHb1 and AHb2 is associated with much smaller enthalpy barriers, described by a distribution peaking at a ΔH_{peak} of 7.9 kJ/mol. These observations resemble those made with MbCO, where CO ligands encounter peak enthalpy barriers of 18.6 (A_3) and 8.7 kJ/mol (A_0) (*64*). Steric effects of the HisE7 side chain in the A substates modulate the energy barriers (*65*): the closer the HisE7 side chain to the heme iron, the higher the barrier at the iron and, therefore, the recombination temperature.

Secondary Docking Sites. Slow-cool illumination has a pronounced effect on the photoproduct spectrum of wt AHb1-CO (Figure 2A, red line). Comparison with the 4 K photoproduct spectrum shows that two new bands have emerged at 2127 and 2140 cm^{-1}, suggesting that at least one additional docking site is accessible to CO ligands. The spectral change is less pronounced for PheB10Leu AHb1-CO (Figure 2B, red line), and no change is visible at all for AHb2-CO (Figure 2C, red line). Apparently, ligand trapping in an additional CO docking site is most efficient in wt AHb1.

In the TDS contour maps obtained after extended illumination, recombination in A_{1921} of AHb1 clearly occurs in two steps (Figure 3C). A minor fraction of the ligands still rebinds from the primary docking site B at ~60 K, but the majority returns from another site at 140 K, which we denote as site C. Rebinding in high-frequency bands A_{1959} and A_{1968} is essentially unchanged. To amplify the changes in the recombination behavior due to the different illumination protocols, we have calculated the difference between the two maps plotted in panels A and C of Figure 3 (Figure 3E). After slow-cool illumination, the extent of rebinding at ~60 K has decreased, as indicated by the red contours, and increased at ~140 K (black contours). Minute effects are also seen for A_{1959}; no difference signal related to A_{1968} is visible.

The photoproduct map (Figure 3D) obtained after slow cooling displays two rather narrow features at 2127 and 2140 cm^{-1}, which span the entire temperature range from 4 to 160 K. From 30 to 80 K, the contours at 2127 cm^{-1} are broadened due to residual rebinding from site B, best seen from the black contours at ~60 K in the difference map in Figure 3F. The red and black contours at ~10 K (Figure 3D) that appear like mirror images again represent ligand reorientation within a docking site.

To exclusively populate ligand docking site C, the slow-cool protocol was modified such that the photolysis laser was switched off at 100 K and the remainder of the cooling to 4 K was done in the dark. This procedure ensures that rebinding from site B happens during cooling of the sample in the dark, and only those ligands that, during the illumination phase, were trapped at sites with high barriers against rebinding remain photolyzed and contribute to the TDS signal. The resulting A state TDS map (Figure 3G) indeed displays only rebinding in A_{1921} at 140 K. The corresponding photoproduct map, however, displays absorption changes in the photoproduct bands at 2127 and 2140 cm^{-1} starting from the lowest temperatures (Figure 3H). A similar observation has been made with an MbCO mutant and analyzed in detail (*27*, *42*). The loss in absorption up to ~100 K is not related to rebinding but rather to librational motions of the CO, which can assume two opposite orientations at site C.

Rebinding of CO from the different docking sites in heme proteins is often visible from discrete steps in kinetic experiments (*63*, *66*−*68*). Interestingly, flash photolysis experiments with AHb1-CO in highly viscous solvents performed in the visible region also showed multiple kinetic features (*69*). However, the rebinding processes observed in the TDS contour plots (Figure 3) cannot be unambiguously assigned to kinetic features in flash photolysis data recorded in the visible region. The kinetics are governed by barriers for rebinding at the heme iron and barriers for migration between different docking sites, which generally vary between the different A conformations. Experiments in the visible, however, do not distinguish between these conformations.

We have also investigated NO migration in AHb1 with FTIR-TDS. After a 10 s illumination, NO ligands rebind at 18 K; slow-cool illumination shifts the temperature of maximal rebinding to ~20 K (Figure S1B of the Supporting Information). In addition, recombination is stretched out to ~100 K, indicating that states with higher recombination barriers have become populated. However, no distinct second rebinding maximum has developed, which suggests that site C is not accessible to NO in AHb1. In contrast, essentially all NO ligands can be trapped in site C after slow-cool illumination of MbNO (*70*).

After the slow cooling of PheB10Leu AHb1-CO under light, additional weak contours associated with A_{1964} are noticeable at 100 K, indicating that, in the A_{1964} substate, only a small fraction of ligands have migrated to site C (Figure 4C). The photoproduct map (Figure 3D) displays an extension of the corresponding feature at 2130 cm^{-1} (Figure 3B) toward higher temperatures. Rebinding in A_{1919} occurs with two populations at ~70 and ~140 K. Thus, in A_3, ligands have become trapped at site C, where they give rise to a doublet of bands at 2128 and 2145 cm^{-1} (Figure 4D). The black contours at ~2145 cm^{-1} and 15 K indicate that CO ligands rotate in site C. Reorientation in B_{2118} at 15 K is absent under slow-cool illumination. Apparently, CO molecules in site B are maintained in the thermodynamically favored orientation under these conditions.

The maps of AHb2-CO generated after slow-cool illumination from 160 to 4 K do not show any discrete additional features as compared to those taken after a 10 s illumination (Figure 5C,D), which implies that secondary sites are essentially inaccessible to ligands in AHb2-CO. Comparison with the contour map after brief illumination (Figure 5A) shows, however, a tail extending to higher temperatures for the TDS feature of A_{1955}. Similar effects were observed for MbCO, where extended illumination at 25 K ("pumping") altered the barrier distribution for ligands rebinding from site B (*43*). The modified CO rebinding under light irradiation not only can arise from ligand migration but also can reflect light-induced changes of the barrier to the heme iron. The inability to populate a second transient docking site in AHb2 is in line with observations from room-temperature flash photolysis experiments in high-viscosity solvents, where kinetic signatures of ligand migration to alternate docking sites were entirely absent (*71*).

Our FTIR-TDS data reveal that only A_3-like AHb molecules can efficiently trap CO ligands at a secondary site C (Figures 3C and 4C). Rebinding from this site in the A_3 conformations of AHb1 and PheB10Leu AHb1 occurs at ~140 K. Most likely, site C in AHb corresponds to site C in the back of the distal pocket in Mb (*68*, *72*, *73*), which is secluded from site B by residue B10. This assignment is supported by the observation that the photoproduct bands of wt and PheB10Leu AHb1 differ in their stretching frequencies (2127 and 2140 cm^{-1} for AHb1 and 2128 and 2145 cm^{-1} for PheB10Leu AHb1), indicating modified interactions. In the A_0-like conformations of AHb1-CO, CO molecules do not populate secondary site C. This behavior is different from that of MbCO, where at least a small fraction of CO molecules reaches docking sites C and D in the A_0 conformation (*43*). The TDS maps of AHb2-CO, which solely exists in a single conformation, do not display a spectral signature of rebinding from an alternative docking site (Figure 5).

Implications for Possible Functions. The UV−visible absorption spectra of the AHb proteins show that ferrous AHb2 is fully hexacoordinated in the absence of exogenous ligands, whereas deoxy AHb1 is a mixture of hexa- and pentacoordinated species. The higher affinity for the endogenous HisE7 imidazole in AHb2 arises from a higher HisE7 on rate, whereas the off rates are essentially identical (*46*). Molecular dynamics studies suggest that these differences may arise from different flexibilities of the polypeptide chains (F. Spyrakis and F. J. Luque, personal communication). In particular, the CD loop is much more flexible in the case of AHb2 and facilitates the pistonlike movement of helix E to allow binding of HisE7 to the heme iron. This same movement, just in the opposite direction, would also explain the apolar environment, leading to a high stretching frequency of heme-bound CO in AHb2-CO after photolysis at 4 K.

Nanosecond laser flash photolysis experiments at 290 K have provided insights into the ligand binding process in AHb1 and AHb2 at physiological temperatures (*46*, *71*, *74*). In AHb1-CO, the initially generated pentacoordinate species rebinds CO in a bimolecular process (at 1 atm of CO, corresponding to 1 mM CO in the solvent) before HisE7 can coordinate to the iron, with a k'_{CO} of 1.22 $\mu M^{-1} s^{-1}$. In AHb2, ~30% of the CO ligands rebind geminately. Subsequently, HisE7 and CO ligands reentering from the solvent compete for the binding site, with a k'_{CO} of 29.9 $\mu M^{-1} s^{-1}$ (*46*). At 1 atm of CO and 290 K, $<5\%$ of the AHb2 molecules bind HisE7. This fraction increases to ~70% once the CO concentration is similar to the protein concentration used in the experiment (~10 μM). In a final step, HisE7 is replaced with CO. This step is rate-limited by HisE7 dissociation [$k_{offHis} = 12\ s^{-1}$ (*46*)].

In this work, we have observed that two different conformational substates predominate in AHb1-CO, which we call A_0-like and A_3-like in accordance with those found in MbCO. In the latter protein, these two subconformations have markedly different ligand binding kinetics (*55*, *63*) because of two effects.

(i) The HisE7 imidazole sterically interferes with ligand binding to the heme iron when it resides inside the heme pocket in A_1 and A_3, and (ii) the HisE7 side chain opens a channel to the outside when it is in the A_0 conformation so that ligand entry and exit may be facilitated (*75*). In general, they both affect the rates of physiological ligand binding and are difficult to entangle because the substates interconvert on the microsecond time scale (*63*, *76*).

Comparison of the FTIR data presented here with the CO rebinding kinetics of the wt, PheB10Leu, and HisE7Leu AHb1 proteins shows the pronounced influence of HisE7 on the binding kinetics. The higher the relative fraction of A_0-like molecules (~10% for wt, ~60% for PheB10Leu, and 100% for HisE7Leu), the higher the ligand association rate coefficient [k'_{CO}(wt) = 1.22 μM^{-1} s^{-1}, k'_{CO}(PheB10Leu) = 5.17 μM^{-1} s^{-1}, and k'_{CO}(HisE7Leu) = 36.6 μM^{-1} s^{-1}] (*54*). AHb2-CO also exists exclusively in a conformation in which the HisE7 imidazole does not sterically hinder ligands and, consequently, exhibits fast bimolecular association kinetics (k'_{CO} = 29.9 μM^{-1} s^{-1}).

The enthalpy barrier distributions corresponding to A_0 and A_3 in AHb1 differ markedly. The increase in the enthalpy barriers of A_3 by ~5−10 kJ/mol with respect to A_0 accounts for a change in the room-temperature association rate by factors of 7−50 and thus contributes to the observed factor of 30 (wt vs HisE7Leu) to a major extent. In addition, ligand exit and entry may also be facilitated in the A_0 conformation. However, we note that the geminate yield increases with the A_0 fraction in flash photolysis experiments with AHb1 (*54*), indicating that the effect of enhanced geminate rebinding from site B due to the low enthalpy barriers in A_0 is not balanced by an enhanced escape due to an open exit channel.

The conformation of the HisE7 imidazole has an additional consequence in AHb1-CO: it also controls ligand migration within the protein. Our results show that CO ligands can be trapped efficiently at secondary ligand docking site C only in A_3. Presumably, migration of the ligand from B to C requires a sufficient residence time in B to occur with a reasonable yield. This finding agrees well with ligand migration studies of wt MbCO, in which only a small fraction of ligands can be trapped at site C in the A_0 conformation (*43*). In Mb mutant HisE7Leu, ~50% of all ligands are found in site C; site D is not populated (*70*). This steric effect of HisE7 apparently does not play a role in binding of NO to AHb1. In both A_3 and A_0, rebinding barriers are very low, and we were not able to populate site C to any detectable extent.

For Mb, internal cavities have been suggested to act as reservoirs to efficiently supply NO to the oxyferrous protein, thus increasing the turnover for NO oxidation (*77*, *78*). At cryogenic temperatures, it was not possible to trap NO in site C of AHb1, which may be a potential NO storage site. Molecular simulations on ligand migration in AHb1 have shown, however, that binding of O_2 facilitates the formation of a pathway through the protein leading from the distal cavity to the bulk solvent (*46*). This pathway could enable NO to settle in site C, approach the bound O_2, and react to the harmless NO_3^-. For AHb2, the lack of secondary docking sites for the photodissociated CO, both at cryogenic and physiological temperatures, strongly suggests that this protein is not involved in NO dioxygenase reactions, at least by means of a mechanism that relies on the supply of the secondary metabolite from internal storage sites.

SUMMARY AND CONCLUSIONS

The stretching spectra of heme-bound CO have revealed pronounced differences in the active site properties of AHb1-CO and AHb2-CO. In AHb1-CO, the spectrum is dominated by high- and low-frequency, A_0- and A_3-type stretching bands. At physiological pH, the HisE7 side chain is in close contact with the CO ligand in the majority A_3-type conformation. In contrast, there is only a single, high-frequency CO band in AHb2-CO, which clearly shows that the HisE7 side chain does not interact with the ligand in this protein.

Geminate CO rebinding from docking site B near the heme iron of wt and mutant PheB10Leu AHb1-CO proteins occurs at much higher temperatures in the A_3 conformation than in the A_0 conformation. Analysis of the temperature dependence in terms of enthalpy barriers yields two Gaussians centered at 13.5 and 18.3 kJ/mol for A_3, whereas the A_0 barriers can be modeled by a single Gaussian centered at 7.9 kJ/mol. This value is also obtained for the barrier in AHb2-CO. On the basis of previous studies with MbCO, we attribute the differences between A_0 and A_3 mainly to steric conflicts exerted by the HisE7 side chain that constrain ligand access to the heme iron. Because of their different rebinding properties, the population ratio of A_0 and A_3 governs the kinetics at room temperature.

Our FTIR-TDS measurements reveal that only A_3-like AHb molecules can efficiently trap CO at a secondary site C (Figures 3C and 4C), from where the ligands rebind at ~140 K. Site C in AHb most likely corresponds to site C in the back of the distal pocket in Mb (*68*, *72*, *73*), which is secluded from site B by residue B10. In the A_0-like conformations of AHb1-CO, CO molecules do not populate secondary site C. AHb2-CO does not display a spectral signature of rebinding from an alternative docking site (Figure 5). In recent reviews, plant Hbs have been assigned to different classes based on the CO stretching frequency, the oxygen affinity, and the extent of hexacoordination (*52*, *79*, *80*). This study adds another criterion to the classification of plant Hbs, i.e., the accessibility of secondary docking sites. The different ligand migration properties suggest that AHb1 may play a role in NO oxidation, whereas this function appears rather unlikely for AHb2.

In this work, we have employed FTIR spectroscopy at cryogenic temperatures to analyze ligand migration and binding in hemoglobins. This approach has clear experimental advantages: rate processes in proteins are thermally activated and can, therefore, be slowed when the temperature is lowered so that we can perform essentially steady-state experiments with an excellent signal-to-noise ratio. In addition, by proper choice of temperature and illumination protocols, reaction intermediates can be enhanced and studied in detail (*43*−*45*). Temperature-dependent changes in spectral bands also provide a wealth of additional information about protein dynamics (*81*, *82*) as well as ligand dynamics and binding (*27*, *31*). While a large number of low-temperature studies of rate processes in proteins exist in the literature that have contributed enormously to our understanding of protein dynamics and function, some researchers may still argue that the results of low-temperature studies are of limited or no relevance for the physiological function of a protein. However, ligand binding in heme proteins, especially Mb, is a particularly vivid example for the relevance of low-temperature studies (*24*−*26*, *31*, *47*, *68*, *83*), which helped elucidate protein−ligand interactions long before these processes could be observed with fast time-resolved experiments at physiological temperatures (*73*, *84*−*88*).

SUPPORTING INFORMATION AVAILABLE

FTIR photolysis difference spectra of ferric AHb1-NO and temperature dependence of the integrated absorption changes calculated from the TDS data of AHb1-CO and ferric AHb1-NO. This material is available free of charge via the Internet at http://pubs.acs.org.

REFERENCES

1. Trevaskis, B., Watts, R. A., Andersson, C. R., Llewellyn, D. J., Hargrove, M. S., Olson, J. S., Dennis, E. S., and Peacock, W. J. (1997) Two hemoglobin genes in *Arabidopsis thaliana*: The evolutionary origins of leghemoglobins. *Proc. Natl. Acad. Sci. U.S.A. 94*, 12230–12234.
2. Duff, S. M., Wittenberg, J. B., and Hill, R. D. (1997) Expression, purification, and properties of recombinant barley (*Hordeum* sp.) hemoglobin. Optical spectra and reactions with gaseous ligands. *J. Biol. Chem. 272*, 16746–16752.
3. Arredondo-Peter, R., Hargrove, M. S., Sarath, G., Moran, J. F., Lohrman, J., Olson, J. S., and Klucas, R. V. (1997) Rice hemoglobins. Gene cloning, analysis, and O_2-binding kinetics of a recombinant protein synthesized in *Escherichia coli*. *Plant Physiol. 115*, 1259–1266.
4. Hunt, P. W., Watts, R. A., Trevaskis, B., Llewelyn, D. J., Burnell, J., Dennis, E. S., and Peacock, W. J. (2001) Expression and evolution of functionally distinct haemoglobin genes in plants. *Plant Mol. Biol. 47*, 677–692.
5. Wittenberg, J. B., Bolognesi, M., Wittenberg, B. A., and Guertin, M. (2002) Truncated hemoglobins: A new family of hemoglobins widely distributed in bacteria, unicellular eukaryotes, and plants. *J. Biol. Chem. 277*, 871–874.
6. Perazzolli, M., Dominici, P., Romero-Puertas, M. C., Zago, E., Zeier, J., Sonoda, M., Lamb, C., and Delledonne, M. (2004) *Arabidopsis* nonsymbiotic hemoglobin AHb1 modulates nitric oxide bioactivity. *Plant Cell 16*, 2785–2794.
7. Olson, J. S., Mathews, A. J., Rohlfs, R. J., Springer, B. A., Egeberg, K. D., Sligar, S. G., Tame, J., Renaud, J. P., and Nagai, K. (1988) The role of the distal histidine in myoglobin and haemoglobin. *Nature 336*, 265–266.
8. Olson, J. S., and Phillips, G. N., Jr. (1996) Kinetic pathways and barriers for ligand binding to myoglobin. *J. Biol. Chem. 271*, 17593–17596.
9. Gardner, P. R., Gardner, A. M., Martin, L. A., and Salzman, A. L. (1998) Nitric oxide dioxygenase: An enzymic function for flavohemoglobin. *Proc. Natl. Acad. Sci. U.S.A. 95*, 10378–10383.
10. Arredondo-Peter, R., Hargrove, M. S., Moran, J. F., Sarath, G., and Klucas, R. V. (1998) Plant hemoglobins. *Plant Physiol. 118*, 1121–1125.
11. Arcovito, A., Benfatto, M., Cianci, M., Hasnain, S. S., Nienhaus, K., Nienhaus, G. U., Savino, C., Strange, R. W., Vallone, B., and Della Longa, S. (2007) X-ray structure analysis of a metalloprotein with enhanced active-site resolution using in situ X-ray absorption near edge structure spectroscopy. *Proc. Natl. Acad. Sci. U.S.A. 104*, 6211–6216.
12. Ormos, P., Szaraz, S., Cupane, A., and Nienhaus, G. U. (1998) Structural factors controlling ligand binding to myoglobin: A kinetic hole-burning study. *Proc. Natl. Acad. Sci. U.S.A. 95*, 6762–6767.
13. Li, T., Quillin, M. L., Phillips, G. N., Jr., and Olson, J. S. (1994) Structural determinants of the stretching frequency of CO bound to myoglobin. *Biochemistry 33*, 1433–1446.
14. Nienhaus, K., Olson, J. S., Franzen, S., and Nienhaus, G. U. (2005) The Origin of Stark splitting in the initial photoproduct state of MbCO. *J. Am. Chem. Soc. 127*, 40–41.
15. Ray, G. B., Li, X.-Y., Ibers, J. A., Sessler, J. L., and Spiro, G. S. (1994) How far can proteins bend the FeCO unit. *J. Am. Chem. Soc. 116*, 162–176.
16. Meuwly, M. (2006) On the influence of the local environment on the CO stretching frequencies in native myoglobin: Assignment of the B-states in MbCO. *ChemPhysChem 7*, 2061–2063.
17. Nutt, D. R., and Meuwly, M. (2004) CO migration in native and mutant myoglobin: Atomistic simulations for the understanding of protein function. *Proc. Natl. Acad. Sci. U.S.A. 101*, 5998–6002.
18. Plattner, N., and Meuwly, M. (2008) The role of higher CO-multipole moments in understanding the dynamics of photodissociated carbonmonoxide in myoglobin. *Biophys. J. 94*, 2505–2515.
19. Kushkuley, B., and Stavrov, S. S. (1997) Theoretical study of the electrostatic and steric effects on the spectroscopic characteristics of the metal-ligand unit of heme proteins. 2. C-O vibrational frequencies, ^{17}O isotropic chemical shifts, and nuclear quadrupole coupling constants. *Biophys. J. 72*, 899–912.
20. Kaposi, A. D., Vanderkooi, J. M., Wright, W. W., Fidy, J., and Stavrov, S. S. (2001) Influence of static and dynamic disorder on the visible and infrared absorption spectra of carbonmonoxy horseradish peroxidase. *Biophys. J. 81*, 3472–3482.
21. Elber, R., and Karplus, M. (1987) Multiple conformational states of proteins: A molecular dynamics analysis of myoglobin. *Science 235*, 318–321.
22. Dalosto, S. D., Vanderkooi, J. M., and Sharp, K. A. (2004) Vibrational Stark Effects on Carbonyl, Nitrile, and Nitrosyl Compounds Including Heme Ligands, CO, CN, and NO, Studied with Density Functional Theory. *J. Phys. Chem. B 108*, 6450–6457.
23. Nienhaus, G. U., Chu, K., and Jesse, K. (1998) Structural heterogeneity and ligand binding in carbonmonoxy myoglobin crystals at cryogenic temperatures. *Biochemistry 37*, 6819–6823.
24. Nienhaus, K., Deng, P., Kriegl, J. M., and Nienhaus, G. U. (2003) Structural Dynamics of Myoglobin: The Effect of Internal Cavities on Ligand Migration and Binding. *Biochemistry 42*, 9647–9658.
25. Nienhaus, K., Deng, P., Kriegl, J. M., and Nienhaus, G. U. (2003) Structural Dynamics of Myoglobin: Spectroscopic and Structural Characterization of Ligand Docking Sites in Myoglobin Mutant L29W. *Biochemistry 42*, 9633–9646.
26. Nienhaus, K., Deng, P., Olson, J. S., Warren, J. J., and Nienhaus, G. U. (2003) Structural Dynamics of Myoglobin: Ligand Migration and Binding in Valine 68 Mutants. *J. Biol. Chem. 278*, 42532–42544.
27. Kriegl, J. M., Nienhaus, K., Deng, P., Fuchs, J., and Nienhaus, G. U. (2003) Ligand dynamics in a protein internal cavity. *Proc. Natl. Acad. Sci. U.S.A. 100*, 7069–7074.
28. Park, E. S., Andrews, S. S., Hu, R. B., and Boxer, S. G. (1999) Vibrational stark spectroscopy in proteins: A probe and calibration for electrostatic fields. *J. Phys. Chem. B 103*, 9813–9817.
29. Hush, N. S., and Reimers, J. R. (1995) Vibrational stark spectroscopy. 1. Basic theory and application to the CO stretch. *J. Phys. Chem. 99*, 15798–15805.
30. Park, E. S., and Boxer, S. G. (2002) Origins of the sensitivity of molecular vibrations on electric fields: Carbonyl and Nitrosyl Stretches in Model Compounds and Proteins. *J. Phys. Chem. B 106*, 5800–5806.
31. Alben, J. O., Beece, D., Bowne, S. F., Doster, W., Eisenstein, L., Frauenfelder, H., Good, D., McDonald, J. D., Marden, M. C., Moh, P. P., Reinisch, L., Reynolds, A. H., Shyamsunder, E., and Yue, K. T. (1982) Infrared spectroscopy of photodissociated carboxymyoglobin at low temperatures. *Proc. Natl. Acad. Sci. U.S.A. 79*, 3744–3748.
32. Yang, F., and Phillips, G. N., Jr. (1996) Crystal structures of CO-, deoxy- and met-myoglobins at various pH values. *J. Mol. Biol. 256*, 762–774.
33. Vojtechovsky, J., Chu, K., Berendzen, J., Sweet, R. M., and Schlichting, I. (1999) Crystal structures of myoglobin-ligand complexes at near-atomic resolution. *Biophys. J. 77*, 2153–2174.
34. Müller, J. D., McMahon, B. H., Chien, E. Y., Sligar, S. G., and Nienhaus, G. U. (1999) Connection between the taxonomic substates and protonation of histidines 64 and 97 in carbonmonoxy myoglobin. *Biophys. J. 77*, 1036–1051.
35. Braunstein, D. P., Chu, K., Egeberg, K. D., Frauenfelder, H., Mourant, J. R., Nienhaus, G. U., Ormos, P., Sligar, S. G., Springer, B. A., and Young, R. D. (1993) Ligand binding to heme proteins: III. FTIR studies of His-E7 and Val-E11 mutants of carbonmonoxymyoglobin. *Biophys. J. 65*, 2447–2454.
36. Nienhaus, K., and Nienhaus, G. U. (2007) Influence of Distal Residue B10 on the CO Dynamics in Myoglobin and Neuroglobin. *J. Biol. Phys. 33*, 357–379.
37. Lamb, D. C., Nienhaus, K., Arcovito, A., Draghi, F., Miele, A. E., Brunori, M., and Nienhaus, G. U. (2002) Structural dynamics of myoglobin: Ligand migration among protein cavities studied by Fourier transform infrared/temperature derivative spectroscopy. *J. Biol. Chem. 277*, 11636–11644.
38. Gibson, Q. H., and Ainsworth, S. (1957) Photosensitivity of haem compounds. *Nature 180*, 1416–1417.
39. Frauenfelder, H., Nienhaus, G. U., and Johnson, J. B. (1991) Rate Processes in Proteins. *Phys. Chem. Chem. Phys. 95*, 272–278.
40. Parak, F. G., and Nienhaus, G. U. (2002) Myoglobin, a Paradigm in the Study of Protein Dynamics. *ChemPhysChem 3*, 249–254.
41. Lim, M., Jackson, T. A., and Anfinrud, P. A. (1997) Ultrafast rotation and trapping of carbon monoxide dissociated from myoglobin. *Nat. Struct. Biol. 4*, 209–214.
42. Lehle, H., Kriegl, J. M., Nienhaus, K., Deng, P., Fengler, S., and Nienhaus, G. U. (2005) Probing electric fields in protein cavities by

using the vibrational Stark effect of carbon monoxide. *Biophys. J. 88*, 1978–1990.
43. Nienhaus, G. U., Mourant, J. R., Chu, K., and Frauenfelder, H. (1994) Ligand binding to heme proteins: The effect of light on ligand binding in myoglobin. *Biochemistry 33*, 13413–13430.
44. Nienhaus, G. U., Mourant, J. R., and Frauenfelder, H. (1992) Spectroscopic evidence for conformational relaxation in myoglobin. *Proc. Natl. Acad. Sci. U.S.A. 89*, 2902–2906.
45. Chu, K., Ernst, R. M., Frauenfelder, H., Mourant, J. R., Nienhaus, G. U., and Philipp, R. (1995) Light-induced and thermal relaxation in a protein. *Phys. Rev. Lett. 74*, 2607–2610.
46. Bruno, S., Faggiano, S., Spyrakis, F., Mozzarelli, A., Abbruzzetti, S., Grandi, E., Viappiani, C., Feis, A., Mackowiak, S., Smulevich, G., Cacciatori, E., and Dominici, P. (2007) The reactivity with CO of AHb1 and AHb2 from *Arabidopsis thaliana* is controlled by the distal HisE7 and internal hydrophobic cavities. *J. Am. Chem. Soc. 129*, 2880–2889.
47. Berendzen, J., and Braunstein, D. (1990) Temperature-derivative spectroscopy: A tool for protein dynamics. *Proc. Natl. Acad. Sci. U.S.A. 87*, 1–5.
48. Mourant, J. R., Braunstein, D. P., Chu, K., Frauenfelder, H., Nienhaus, G. U., Ormos, P., and Young, R. D. (1993) Ligand binding to heme proteins: II. Transitions in the heme pocket of myoglobin. *Biophys. J. 65*, 1496–1507.
49. Bredenbeck, J., Helbing, J., Nienhaus, K., Nienhaus, G. U., and Hamm, P. (2007) Protein ligand migration mapped by nonequilibrium 2D-IR exchange spectroscopy. *Proc. Natl. Acad. Sci. U.S.A. 104*, 14243–14248.
50. Nienhaus, K., Maes, E. M., Weichsel, A., Montfort, W. R., and Nienhaus, G. U. (2004) Structural dynamics controls nitric oxide affinity in nitrophorin 4. *J. Biol. Chem. 279*, 39401–39407.
51. Vogel, K. M., Kozlowski, P. M., Zgierski, M. Z., and Spiro, T. G. (1999) Determinants of the FeXO (X = C, N, O) vibrational frequencies in heme adducts from experiment and density functional theory. *J. Am. Chem. Soc. 121*, 9915–9921.
52. Hoy, J. A., Robinson, H., Trent, J. T., III, Kakar, S., Smagghe, B. J., and Hargrove, M. S. (2007) Plant hemoglobins: A molecular fossil record for the evolution of oxygen transport. *J. Mol. Biol. 371*, 168–179.
53. Spiro, T. G., and Wasbotten, I. H. (2005) CO as a vibrational probe of heme protein active sites. *J. Inorg. Biochem. 99*, 34–44.
54. Faggiano, S., Abbruzzetti, S., Spyrakis, F., Grandi, E., Viappiani, C., Bruno, S., Mozzarelli, A., Cozzini, P., Astegno, A., Dominici, P., Brogioni, S., Feis, A., Smulevich, G., Carrillo, O., Schmidtke, P., Bidon-Chanal, A., and Luque, F. J. (2009) Structural Plasticity and Functional Implications of Internal Cavities in Distal Mutants of Type 1 Non-Symbiotic Hemoglobin AHb1 from *Arabidopsis thaliana*. *J. Phys. Chem. B 113*, 16028–16038.
55. Young, R. D., Frauenfelder, H., Johnson, J. B., Lamb, D. C., Nienhaus, G. U., Phillip, R., and Scholl, R. (1991) Time- and temperature dependence of large-scale conformational transitions in myoglobin. *Chem. Phys. 158*, 315–328.
56. Park, K. D., Guo, K. M., Adebodun, F., Chiu, M. L., Sligar, S. G., and Oldfield, E. (1991) Distal and proximal ligand interactions in heme proteins: Correlations between C-O and Fe-C vibrational frequencies, oxygen-17 and carbon-13 nuclear magnetic resonance chemical shifts, and oxygen-17 nuclear quadrupole coupling constants in $C^{17}O$- and ^{13}CO-labeled species. *Biochemistry 30*, 2333–2347.
57. Smagghe, B. J., Kundu, S., Hoy, J. A., Halder, P., Weiland, T. R., Savage, A., Venugopal, A., Goodman, M., Premer, S., and Hargrove, M. S. (2006) Role of phenylalanine B10 in plant nonsymbiotic hemoglobins. *Biochemistry 45*, 9735–9745.
58. Teng, T. Y., Srajer, V., and Moffat, K. (1994) Photolysis-induced structural changes in single crystals of carbonmonoxy myoglobin at 40 K. *Nat. Struct. Biol. 1*, 701–705.
59. Hartmann, H., Zinser, S., Komninos, P., Schneider, R. T., Nienhaus, G. U., and Parak, F. (1996) X-ray structure determination of a metastable state of carbonmonoxy myoglobin after photodissociation. *Proc. Natl. Acad. Sci. U.S.A. 93*, 7013–7016.
60. Schlichting, I., Berendzen, J., Phillips, G. N., Jr., and Sweet, R. M. (1994) Crystal structure of photolysed carbonmonoxy-myoglobin. *Nature 371*, 808–812.
61. Lutz, S., Nienhaus, K., Nienhaus, G. U., and Meuwly, M. (2009) Ligand migration between internal docking sites in photodissociated carbonmonoxy neuroglobin. *J. Phys. Chem. B 113*, 15334–15343.
62. Nienhaus, K., Lutz, S., Meuwly, M., and Nienhaus, G. U. (2010) Structural identification of spectroscopic substates in neuroglobin. *ChemPhysChem 11*, 119–129.
63. Johnson, J. B., Lamb, D. C., Frauenfelder, H., Müller, J. D., McMahon, B., Nienhaus, G. U., and Young, R. D. (1996) Ligand binding to heme proteins. VI. Interconversion of taxonomic substates in carbonmonoxymyoglobin. *Biophys. J. 71*, 1563–1573.
64. Steinbach, P. J., Ansari, A., Berendzen, J., Braunstein, D., Chu, K., Cowen, B. R., Ehrenstein, D., Frauenfelder, H., Johnson, J. B., Lamb, D. C., Luck, S., Mourant, J. R., Nienhaus, G. U., Ormos, P., Philipp, R., Xie, A., and Young, R. D. (1991) Ligand binding to heme proteins: Connection between dynamics and function. *Biochemistry 30*, 3988–4001.
65. McMahon, B. H., Stojkovic, B. P., Hay, P. J., Martin, R. L., and García, A. E. (2000) Microscopic model of carbon monoxide binding to myoglobin. *J. Chem. Phys. 113*, 6831–6850.
66. Lamb, D. C., Arcovito, A., Nienhaus, K., Minkow, O., Draghi, F., Brunori, M., and Nienhaus, G. U. (2004) Structural dynamics of myoglobin: An infrared kinetic study of ligand migration in mutants YQR and YQRF. *Biophys. Chem. 109*, 41–58.
67. Pesce, A., Nardini, M., Ascenzi, P., Geuens, E., Dewilde, S., Moens, L., Bolognesi, M., Riggs, A. F., Hale, A., Deng, P., Nienhaus, G. U., Olson, J. S., and Nienhaus, K. (2004) ThrE11 regulates O_2 affinity in *Cerebratulus lacteus* mini-hemoglobin. *J. Biol. Chem. 279*, 33662–33672.
68. Ostermann, A., Waschipky, R., Parak, F. G., and Nienhaus, G. U. (2000) Ligand binding and conformational motions in myoglobin. *Nature 404*, 205–208.
69. Abbruzzetti, S., Grandi, E., Bruno, S., Faggiano, S., Spyrakis, F., Mozzarelli, A., Cacciatori, E., Dominici, P., and Viappiani, C. (2007) Ligand migration in nonsymbiotic hemoglobin AHb1 from *Arabidopsis thaliana*. *J. Phys. Chem. B 111*, 12582–12590.
70. Nienhaus, K., Palladino, P., and Nienhaus, G. U. (2008) Structural dynamics of myoglobin: FTIR-TDS study of NO migration and binding. *Biochemistry 47*, 935–948.
71. Bruno, S., Faggiano, S., Spyrakis, F., Mozzarelli, A., Cacciatori, E., Dominici, P., Grandi, E., Abbruzzetti, S., and Viappiani, C. (2007) Different roles of protein dynamics and ligand migration in non-symbiotic hemoglobins AHb1 and AHb2 from *Arabidopsis thaliana*. *Gene 398*, 224–233.
72. Brunori, M., Vallone, B., Cutruzzola, F., Travaglini-Allocatelli, C., Berendzen, J., Chu, K., Sweet, R. M., and Schlichting, I. (2000) The role of cavities in protein dynamics: Crystal structure of a photolytic intermediate of a mutant myoglobin. *Proc. Natl. Acad. Sci. U.S.A. 97*, 2058–2063.
73. Schotte, F., Lim, M., Jackson, T. A., Smirnov, A. V., Soman, J., Olson, J. S., Phillips, G. N., Jr., Wulff, M., and Anfinrud, P. A. (2003) Watching a protein as it functions with 150-ps time-resolved X-ray crystallography. *Science 300*, 1944–1947.
74. Abbruzzetti, S., Bruno, S., Faggiano, S., Grandi, E., Mozzarelli, A., and Viappiani, C. (2006) Time-resolved methods in biophysics. 2. Monitoring haem proteins at work with nanosecond laser flash photolysis. *Photochem. Photobiol. Sci. 5*, 1109–1120.
75. Scott, E. E., Gibson, Q. H., and Olson, J. S. (2001) Mapping the pathways for O_2 entry into and exit from myoglobin. *J. Biol. Chem. 276*, 5177–5188.
76. Young, R. D., and Bowne, S. F. (1984) Conformational substates and barrier height distributions in ligand binding to heme proteins. *J. Chem. Phys. 81*, 3730–3737.
77. Brunori, M. (2001) Nitric oxide moves myoglobin centre stage. *Trends Biochem. Sci. 26*, 209–210.
78. Frauenfelder, H., McMahon, B. H., Austin, R. H., Chu, K., and Groves, J. T. (2001) The role of structure, energy landscape, dynamics, and allostery in the enzymatic function of myoglobin. *Proc. Natl. Acad. Sci. U.S.A. 98*, 2370–2374.
79. Smagghe, B. J., Hoy, J. A., Percifield, R., Kundu, S., Hargrove, M. S., Sarath, G., Hilbert, J. L., Watts, R. A., Dennis, E. S., Peacock, W. J., Dewilde, S., Moens, L., Blouin, G. C., Olson, J. S., and Appleby, C. A. (2009) Review: Correlations between oxygen affinity and sequence classifications of plant hemoglobins. *Biopolymers 91*, 1083–1096.
80. Hoy, J. A., and Hargrove, M. S. (2008) The structure and function of plant hemoglobins. *Plant Physiol. Biochem. 46*, 371–379.
81. Parak, F., Heidemeier, J., and Nienhaus, G. U. (1988) Protein structural dynamics as determined by Mössbauer spectroscopy. *Hyperfine Interact. 40*, 147–158.
82. Doster, W., Cusack, S., and Petry, W. (1989) Dynamical transition of myoglobin revealed by inelastic neutron scattering. *Nature 337*, 754–756.
83. Austin, R. H., Beeson, K. W., Eisenstein, L., Frauenfelder, H., and Gunsalus, I. C. (1975) Dynamics of ligand binding to myoglobin. *Biochemistry 14*, 5355–5373.

84. Lim, M., Jackson, T. A., and Anfinrud, P. A. (1995) Binding of CO to myoglobin from a heme pocket docking site to form nearly linear Fe-C-O. *Science 269*, 962–966.
85. Bourgeois, D., Vallone, B., Schotte, F., Arcovito, A., Miele, A. E., Sciara, G., Wulff, M., Anfinrud, P., and Brunori, M. (2003) Complex landscape of protein structural dynamics unveiled by nanosecond Laue crystallography. *Proc. Natl. Acad. Sci. U.S.A. 100*, 8704–8709.
86. Hummer, G., Schotte, F., and Anfinrud, P. A. (2004) Unveiling functional protein motions with picosecond X-ray crystallography and molecular dynamics simulations. *Proc. Natl. Acad. Sci. U.S.A. 101*, 15330–15334.
87. Schmidt, M., Nienhaus, K., Pahl, R., Krasselt, A., Anderson, S., Parak, F., Nienhaus, G. U., and Srajer, V. (2005) Ligand migration pathway and protein dynamics in myoglobin: a time-resolved crystallographic study on L29W MbCO. *Proc. Natl. Acad. Sci. U.S.A. 102*, 11704–11709.
88. Srajer, V., Teng, T., Ursby, T., Pradervand, C., Ren, Z., Adachi, S., Schildkamp, W., Bourgeois, D., Wulff, M., and Moffat, K. (1996) Photolysis of the carbon monoxide complex of myoglobin: Nanosecond time-resolved crystallography. *Science 274*, 1726–1729.